The Astrophysical Journal, 826:1 (9pp), 2016 July 20 doi:10.3847/0004-637X/826/1/1

FERMI LARGE AREA TELESCOPE DETECTION OF EXTENDED GAMMA-RAY EMISSION FROM THE RADIO GALAXY FORNAX A

M. Ackermann[1], M. Ajello[2], L. Baldini[3,4], J. Ballet[5], G. Barbiellini[6,7], D. Bastieri[8,9], R. Bellazzini[10], E. Bissaldi[11], R. D. Blandford[4], E. D. Bloom[4], R. Bonino[12,13], T. J. Brandt[14], J. Bregeon[15], P. Bruel[16], R. Buehler[1], S. Buson[14,17,18], G. A. Caliandro[4,19], R. A. Cameron[4], M. Caragiulo[20,11], P. A. Caraveo[21], E. Cavazzuti[22], C. Cecchi[23,24], E. Charles[4], A. Chekhtman[25,52], C. C. Cheung[26], G. Chiaro[9], S. Ciprini[22,23], J. M. Cohen[14,27], J. Cohen-Tanugi[15], F. Costanza[11], S. Cutini[22,23], F. D'Ammando[28,29], D. S. Davis[14,17], A. de Angelis[30], F. de Palma[11,31], R. Desiante[12,32], S. W. Digel[4], N. Di Lalla[10], M. Di Mauro[4], L. Di Venere[20,11], C. Favuzzi[20,11], S. J. Fegan[16], E. C. Ferrara[14], W. B. Focke[4], Y. Fukazawa[33], S. Funk[34], P. Fusco[11,20], F. Gargano[11], D. Gasparrini[22,23], M. Georganopoulos[17], N. Giglietto[11,20], F. Giordano[20,11], M. Giroletti[28], G. Godfrey[4], D. Green[14,27], I. A. Grenier[5], S. Guiriec[14,53], E. Hays[14], J. W. Hewitt[35], A. B. Hill[36,4], T. Jogler[4], G. Jóhannesson[37], S. Kensei[33], M. Kuss[10], S. Larsson[38,39], L. Latronico[12], J. Li[40], L. Li[38,39], F. Longo[6,7], F. Loparco[11,20], P. Lubrano[23], J. D. Magill[27], S. Maldera[12], A. Manfreda[10], M. Mayer[1], M. N. Mazziotta[11], W. McConville[14,27], J. E. McEnery[14,27], P. F. Michelson[4], W. Mitthumsiri[41], T. Mizuno[42], M. E. Monzani[4], A. Morselli[43], I. V. Moskalenko[4], S. Murgia[44], M. Negro[12,13], E. Nuss[15], M. Ohno[33], T. Ohsugi[42], M. Orienti[28], E. Orlando[4], J. F. Ormes[45], D. Paneque[4,46], J. S. Perkins[14], M. Pesce-Rollins[10,4], F. Piron[15], G. Pivato[10], T. A. Porter[4], S. Rainò[11,20], R. Rando[8,9], M. Razzano[10,54], A. Reimer[4,47], O. Reimer[4,47], J. Schmid[5], C. Sgrò[10], D. Simone[11], E. J. Siskind[48], F. Spada[10], G. Spandre[10], P. Spinelli[11,20], Ł. Stawarz[49], H. Takahashi[33], J. B. Thayer[4], D. J. Thompson[14], D. F. Torres[40,50], G. Tosti[23,24], E. Troja[14,27], G. Vianello[4], K. S. Wood[26], M. Wood[4], and S. Zimmer[51]

[1] Deutsches Elektronen Synchrotron DESY, D-15738 Zeuthen, Germany
[2] Department of Physics and Astronomy, Clemson University, Kinard Lab of Physics, Clemson, SC 29634-0978, USA
[3] Università di Pisa and Istituto Nazionale di Fisica Nucleare, Sezione di Pisa I-56127 Pisa, Italy
[4] W. W. Hansen Experimental Physics Laboratory, Kavli Institute for Particle Astrophysics and Cosmology, Department of Physics and SLAC National Accelerator Laboratory, Stanford University, Stanford, CA 94305, USA
[5] Laboratoire AIM, CEA-IRFU/CNRS/Université Paris Diderot, Service d'Astrophysique, CEA Saclay, F-91191 Gif sur Yvette, France
[6] Istituto Nazionale di Fisica Nucleare, Sezione di Trieste, I-34127 Trieste, Italy
[7] Dipartimento di Fisica, Università di Trieste, I-34127 Trieste, Italy
[8] Istituto Nazionale di Fisica Nucleare, Sezione di Padova, I-35131 Padova, Italy
[9] Dipartimento di Fisica e Astronomia "G. Galilei," Università di Padova, I-35131 Padova, Italy
[10] Istituto Nazionale di Fisica Nucleare, Sezione di Pisa, I-56127 Pisa, Italy
[11] Istituto Nazionale di Fisica Nucleare, Sezione di Bari, I-70126 Bari, Italy
[12] Istituto Nazionale di Fisica Nucleare, Sezione di Torino, I-10125 Torino, Italy
[13] Dipartimento di Fisica Generale "Amadeo Avogadro," Università degli Studi di Torino, I-10125 Torino, Italy
[14] NASA Goddard Space Flight Center, Greenbelt, MD 20771, USA; wmcconvi@umd.edu
[15] Laboratoire Univers et Particules de Montpellier, Université Montpellier, CNRS/IN2P3, F-34095 Montpellier, France
[16] Laboratoire Leprince-Ringuet, École polytechnique, CNRS/IN2P3, F-91128 Palaiseau, France
[17] Department of Physics and Center for Space Sciences and Technology, University of Maryland Baltimore County, Baltimore, MD 21250, USA; georgano@umbc.edu
[18] Center for Research and Exploration in Space Science and Technology (CRESST) and NASA Goddard Space Flight Center, Greenbelt, MD 20771, USA
[19] Consorzio Interuniversitario per la Fisica Spaziale (CIFS), I-10133 Torino, Italy
[20] Dipartimento di Fisica "M. Merlin" dell'Università e del Politecnico di Bari, I-70126 Bari, Italy
[21] INAF-Istituto di Astrofisica Spaziale e Fisica Cosmica, I-20133 Milano, Italy
[22] Agenzia Spaziale Italiana (ASI) Science Data Center, I-00133 Roma, Italy
[23] Istituto Nazionale di Fisica Nucleare, Sezione di Perugia, I-06123 Perugia, Italy
[24] Dipartimento di Fisica, Università degli Studi di Perugia, I-06123 Perugia, Italy
[25] College of Science, George Mason University, Fairfax, VA 22030, USA
[26] Space Science Division, Naval Research Laboratory, Washington, DC 20375-5352, USA; Teddy.Cheung@nrl.navy.mil.
[27] Department of Physics and Department of Astronomy, University of Maryland, College Park, MD 20742, USA; jmagill@umd.edu
[28] INAF Istituto di Radioastronomia, I-40129 Bologna, Italy
[29] Dipartimento di Astronomia, Università di Bologna, I-40127 Bologna, Italy
[30] Dipartimento di Fisica, Università di Udine and Istituto Nazionale di Fisica Nucleare, Sezione di Trieste, Gruppo Collegato di Udine, I-33100 Udine, Italy
[31] Università Telematica Pegaso, Piazza Trieste e Trento, 48, I-80132 Napoli, Italy
[32] Università di Udine, I-33100 Udine, Italy
[33] Department of Physical Sciences, Hiroshima University, Higashi-Hiroshima, Hiroshima 739-8526, Japan
[34] Erlangen Centre for Astroparticle Physics, D-91058 Erlangen, Germany
[35] University of North Florida, Department of Physics, 1 UNF Drive, Jacksonville, FL 32224 , USA
[36] School of Physics and Astronomy, University of Southampton, Highfield, Southampton, SO17 1BJ, UK
[37] Science Institute, University of Iceland, IS-107 Reykjavik, Iceland
[38] Department of Physics, KTH Royal Institute of Technology, AlbaNova, SE-106 91 Stockholm, Sweden
[39] The Oskar Klein Centre for Cosmoparticle Physics, AlbaNova, SE-106 91 Stockholm, Sweden
[40] Institute of Space Sciences (IEEC-CSIC), Campus UAB, E-08193 Barcelona, Spain
[41] Department of Physics, Faculty of Science, Mahidol University, Bangkok 10400, Thailand
[42] Hiroshima Astrophysical Science Center, Hiroshima University, Higashi-Hiroshima, Hiroshima 739-8526, Japan
[43] Istituto Nazionale di Fisica Nucleare, Sezione di Roma "Tor Vergata," I-00133 Roma, Italy
[44] Center for Cosmology, Physics and Astronomy Department, University of California, Irvine, CA 92697-2575, USA
[45] Department of Physics and Astronomy, University of Denver, Denver, CO 80208, USA
[46] Max-Planck-Institut für Physik, D-80805 München, Germany
[47] Institut für Astro- und Teilchenphysik and Institut für Theoretische Physik, Leopold-Franzens-Universität Innsbruck, A-6020 Innsbruck, Austria

[48] NYCB Real-Time Computing Inc., Lattingtown, NY 11560-1025, USA
[49] Astronomical Observatory, Jagiellonian University, 30-244 Kraków, Poland; stawarz@oa.uj.edu.pl
[50] Institució Catalana de Recerca i Estudis Avançats (ICREA), Barcelona, Spain
[51] University of Geneva, Département de physique nucléaire et corpusculaire (DPNC), 24 quai Ernest-Ansermet, CH-1211 Genève 4, Switzerland
Received 2016 March 23; revised 2016 May 23; accepted 2016 May 28; published 2016 July 14

ABSTRACT

We report the *Fermi* Large Area Telescope detection of extended γ-ray emission from the lobes of the radio galaxy Fornax A using 6.1 years of Pass 8 data. After Centaurus A, this is now the second example of an extended γ-ray source attributed to a radio galaxy. Both an extended flat disk morphology and a morphology following the extended radio lobes were preferred over a point-source description, and the core contribution was constrained to be $<14\%$ of the total γ-ray flux. A preferred alignment of the γ-ray elongation with the radio lobes was demonstrated by rotating the radio lobes template. We found no significant evidence for variability on $\sim$0.5 year timescales. Taken together, these results strongly suggest a lobe origin for the γ-rays. With the extended nature of the >100 MeV γ-ray emission established, we model the source broadband emission considering currently available total lobe radio and millimeter flux measurements, as well as X-ray detections attributed to inverse Compton (IC) emission off the cosmic microwave background (CMB). Unlike the Centaurus A case, we find that a leptonic model involving IC scattering of CMB and extragalactic background light (EBL) photons underpredicts the γ-ray fluxes by factors of about $\sim$2–3, depending on the EBL model adopted. An additional γ-ray spectral component is thus required, and could be due to hadronic emission arising from proton–proton collisions of cosmic rays with thermal plasma within the radio lobes.

Key words: galaxies: active – galaxies: individual (Fornax A) – galaxies: jets – gamma rays: galaxies – radiation mechanisms: non-thermal

1. INTRODUCTION

The radio galaxy Fornax A, well known for its radio lobes spanning $\sim 50'$, with a lobe-to-lobe separation of $\sim 33'$ (see Ekers et al. 1983), is one of the closest and brightest radio galaxies, located at a distance of only 18.6 Mpc (Madore et al. 1999). Hosted by the elliptical galaxy NGC 1316, the radio source contains a low-ionization nuclear emission-line region nucleus, which has been imaged to arcsecond-scale resolution and features a flat spectrum ($\alpha = 0.4$; $S_\nu \propto \nu^{-\alpha}$) core with dual-opposing "s"-shaped jets that are detected out to $\sim$5 kpc from the core (Geldzahler & Fomalont 1984). The radio lobes are characterized by a complex polarized filamentary structure with no observable hotspots (Fomalont et al. 1989).

Fornax A was the first radio galaxy reported to emit diffuse, non-thermal X-ray emission from within its radio lobes from observations with *ROSAT* (Feigelson et al. 1995) and ASCA (Kaneda et al. 1995), which were later confirmed through dedicated observations of the east lobe with *XMM-Newton* (Isobe et al. 2006) and the west lobe with *Suzaku* (Tashiro et al. 2009). The non-thermal X-rays have been widely attributed to inverse Compton (IC) emission of relativistic electrons scattering on cosmic microwave background (CMB) photons, with the same population of relativistic electrons producing both synchrotron and IC emission (e.g., Harris & Grindlay 1979). To date, similar leptonic IC/CMB emission has been detected in X-rays from tens of extended lobes in radio galaxies and quasars. In general, such detections imply that the ratio of relativistic electron pressure to magnetic field pressure within the lobes is $\sim$1–100 (Croston et al. 2005; Kataoka & Stawarz 2005; Isobe et al. 2011). More recently, Seta et al. (2013) reported a detection of thermal emission from the western lobe of Fornax A using combined *Suzaku* and *XMM-Newton* data. Thermal emission in the lobes of a radio galaxy is typically not seen, although evidence for this has also been reported in the giant lobes of the nearby radio galaxy Centaurus A (O'Sullivan et al. 2013; Stawarz et al. 2013).

Motivated by the observed (and presumed IC/CMB) X-ray emission from the lobes of Fornax A, Cheung (2007) predicted that the high-energy tail of the IC/CMB would be detected by the *Fermi* Large Area Telescope (LAT; Atwood et al. 2009) at >100 MeV. Following this, Georganopoulos et al. (2008) predicted that the lobes would also be detected in γ-rays at higher energies by the LAT due to IC upscattering of the infrared and optical extragalactic background light (EBL) photons, analogous to the CMB photons upscattered to X-ray energies. The association of Fornax A with the *Fermi*-LAT second year catalog (hereafter 2FGL; Nolan et al. 2012) source 2FGL J0322.4−3717 thus raised an important question regarding the origin of the γ-ray source, which at the time had no evidence presented for significant extension. In particular, a distinction between emission arising from the lobes and possible contamination from the central core region could not be established from the γ-ray data alone, although X-ray and radio observations (Kim & Fabbiano 2003) suggested that the contribution from the core was likely to be minimal.

In a recent study by McKinley et al. (2015), the spectrum of the Fornax A lobes was modeled in multiple wavelengths using both leptonic and hadronic production scenarios without knowledge of γ-ray spatial extent or γ-ray contamination from the galaxy core. They concluded the most likely source of γ-ray production is hadronic processes within filamentary structures of the lobes. Our study follows the successful γ-ray detection of the extended lobes from Centaurus A (Abdo et al. 2010), and LAT studies of the lobes of NGC 6251 (Takeuchi et al. 2012) and Centaurus B (Katsuta et al. 2013). Gamma-ray upper limits using H.E.S.S. and *Fermi*-LAT observations have been used to constrain the hadronic cosmic-ray population within the radio lobes of Hydra A (Abramowski et al. 2012).

[52] Resident at Naval Research Laboratory, Washington, DC 20375, USA.
[53] NASA Postdoctoral Program Fellow, USA.
[54] Funded by contract FIRB-2012-RBFR12PM1F from the Italian Ministry of Education, University and Research (MIUR).

Fornax A is not associated with a γ-ray source in the most recent, third *Fermi*-LAT catalog based on four years of LAT data (3FGL, Acero et al. 2015; 3LAC, Ackermann et al. 2015). However, the centroid of the source 3FGL J0322.5−3721 is offset by $0.^{\circ}15$ from the core of Fornax A. This offset is greater than the 95% position uncertainty of the 3FGL source. In the following we discuss possible reasons for this offset, detail a significant γ-ray detection of extended emission from Fornax A using 6.1 years of *Fermi*-LAT data, and present modeling under leptonic and hadronic scenarios. Detecting extended emission from Fornax A with the LAT is challenging because the 68% containment point-spread function (PSF) radius is $\sim 0.^{\circ}8$ at 1 GeV, which is larger than the Fornax A lobe-to-lobe separation. The LAT PSF is energy dependent going from 5° at 100 MeV to $0.^{\circ}1$ at 100 GeV with 68% confidence.[55]

2. OBSERVATIONS AND ANALYSIS

2.1. Fermi-LAT Observations

Unlike all studies mentioned in Section 1, we used 6.1 years (from 2008 August 4 to 2014 September 4) of Pass 8 LAT data. Compared to previous iterations of the LAT event-level analysis, Pass 8 provides greater acceptance and a PSF (Sgrò 2014), as well as event type partitions according to PSF[56], which we used in this analysis. All of these factors allowed for a firm detection of extension of Fornax A. We selected from all-sky survey data at energies from 0.1 to 300 GeV extracted from a region of interest (ROI) with 10° radius centered at the J2000.0 radio position of Fornax A (R.A. $= 50.^{\circ}673$, decl. $= -37.^{\circ}208$, Geldzahler & Fomalont 1984). We used the "source" event class, recommended for individual source analysis, a zenith angle limit of 100° to greatly reduce contamination from the Earth limb, and a rocking angle limit of 52°. *Fermi* Science Tools `v10r01p00` and instrument response functions (IRFs) `P8R2_SOURCE_V6` were used for this analysis.[57]

To model the LAT data, we included all sources from the 3FGL within 10° of the radio core position of Fornax A. The diffuse background was modeled using preliminary versions of Galactic diffuse and isotropic spectral templates recommended by the *Fermi*-LAT collaboration, of which the finalized versions have been released to the public.[58] Several tests were performed, and we determined that the results presented here with the preliminary diffuse models are compatible with those obtained with the finalized models. We used the same spectral models as in the 3FGL catalog for all background sources, and the normalization and spectral shape parameters of all point sources were left free during optimization. For the diffuse models, only the normalization parameters were left free.

We initially modeled Fornax A as a point source located at the position of the radio core, removing 3FGL J0322.5−3721 from the model since it is offset from the radio core by $0.^{\circ}15$. We optimized the localization using the `gtfindsrc` tool provided in the Science Tools in unbinned mode. The best-fit localization is R.A. $= 50.^{\circ}73$, decl. $= -37.^{\circ}28$ with a 95% confidence error circle radius of $0.^{\circ}14$, slightly southeast of the position of the Fornax A core and consistent with the reported 3FGL localization. Figure 1 shows the best-fit localization (point B) and the core (point A) as well as the 2FGL and 3FGL error contours plotted on top of the relative residual counts map. Optimizing the model with the single point source at point B, we detect γ-ray emission at a Test Statistic (TS)[59] = 121. The spectrum was modeled as a single power law with a resulting maximum-likelihood photon index $\Gamma = 2.08 \pm 0.08$ and a full band energy flux of $(5.34 \pm 0.78_{\rm stat}{}^{+0.03}_{-0.05}{}_{\rm sys}) \times 10^{-12}$ erg cm^{-2} s^{-1} (see Table 2). Systematic errors are due to the systematic uncertainty in the LAT effective area.[60] These fluxes and indices are consistent with those reported in the catalogs for sources 2FGL J0322.4−3717 and 3FGL J0322.5−3721.

2.2. Extension and Morphology

In the following, we describe several tests performed to determine the morphology of the observed γ-ray emission from the direction of Fornax A, as summarized in Tables 1 and 2. All tests on extension and morphology made full use of the additional spatial information brought about by the new Pass 8 PSF event type partitions. The broadband flux and spectrum optimizations in addition to these tests were performed using all PSF types in composite likelihood.

2.2.1. Spatial Extension

To determine if the γ-ray emission is extended beyond that of a point source we modeled Fornax A as a flat circular disk of various sizes ($0.^{\circ}03$–$0.^{\circ}75$ in steps of $0.^{\circ}03$) by producing several disk templates centered at the best-fit location of the LAT source described in Section 2.1 (point B in Figure 1). The uniform disk is the simplest spatial model, and the use of a Gaussian profile has typically been shown to produce comparatively little difference in the overall likelihood and best-fit spectral parameters (Lande et al. 2012). Using `gtlike` in binned mode (with bin size $0.^{\circ}05$), we determined the overall likelihood $\mathcal{L}$ as a function of the disk radius r. As shown in Figure 2(a), $\mathcal{L}$ is peaked at $r = 0.^{\circ}33 \pm 0.^{\circ}05$, which is roughly compatible with the extent of the lobes as observed in radio (1.5 GHz at $14''$ resolution, Fomalont et al. 1989). By comparing the likelihood of the peak radius with the near-zero radius of $0.^{\circ}03$ (effectively a point source), we found that the γ-ray emission is spatial extended with 5.9σ confidence ($\Delta \log \mathcal{L} = 17.3$, 1 degree of freedom, Wilks 1938). See Tables 1 and 2 for more information.

2.2.2. Blind Tests for Morphology

With the aim of making no prior assumptions about the morphology of the γ-ray emission in this region, we used the ROI fit with our position-optimized point source as described in Section 2.1 and removed that point source from the model, thereby leaving only the background sources. Using this background model, we created a map of residual counts above 1 GeV in the ROI by subtracting the model's predicted counts from the observed counts in each bin. Apart from the emission near Fornax A, the map of residuals is flat in significance and

[55] http://www.slac.stanford.edu/exp/glast/groups/canda/lat_Performance.htm
[56] http://fermi.gsfc.nasa.gov/ssc/data/analysis/LAT_essentials.html
[57] http://fermi.gsfc.nasa.gov/ssc/data/analysis/software
[58] http://fermi.gsfc.nasa.gov/ssc/data/access/lat/BackgroundModels.html
[59] TS is defined as twice the difference between the logarithmic likelihood of the null hypothesis $\mathcal{L}_0$ and the alternative hypothesis being tested $\mathcal{L}_1$ (Mattox et al. 1996): TS $= 2(\log \mathcal{L}_1 - \log \mathcal{L}_0)$.
[60] http://fermi.gsfc.nasa.gov/ssc/data/analysis/LAT_caveats.html

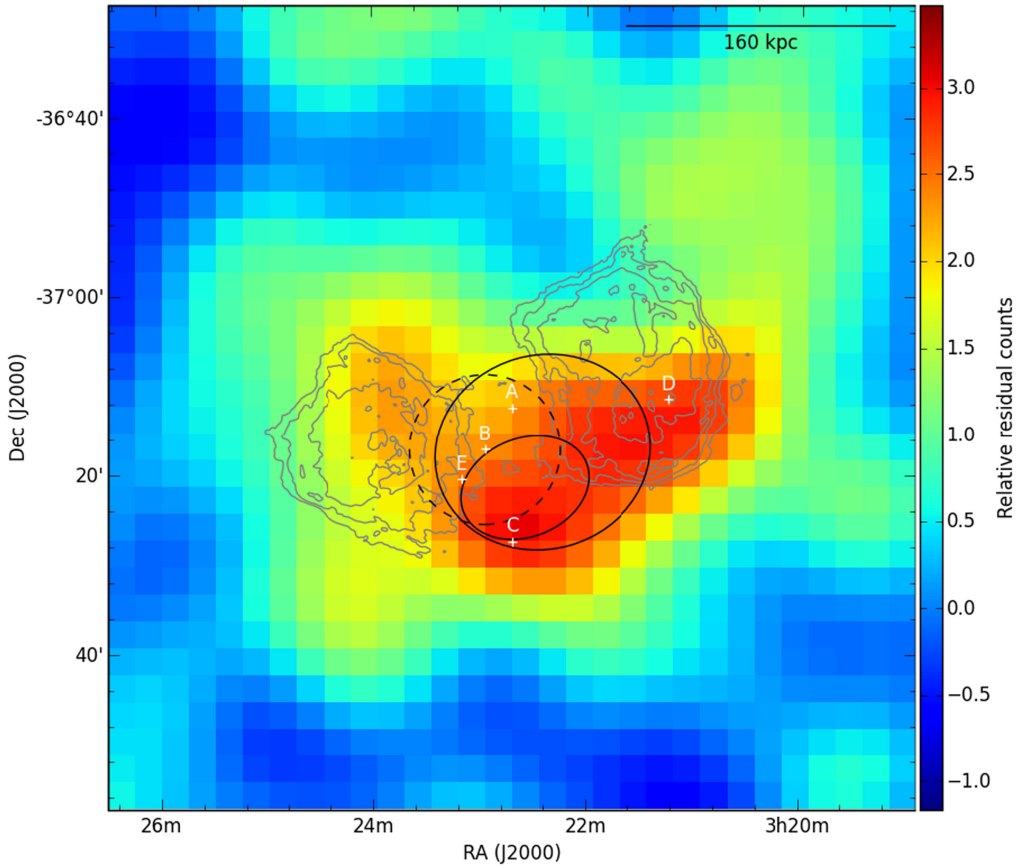

Figure 1. Relative smoothed (4.7 px, 0.°24 Gaussian FWHM) residual γ-ray counts ((counts-model)/model) in the 1.°5 square region around the core of Fornax A between 1 and 300 GeV. Overlaid are the radio contours (gray lines) from the VLA observations of Fomalont et al. (1989) with the radio core (position indicated by A) subtracted. The γ-ray residual counts are elongated in a similar way to the radio lobes. Also shown are the 95% confidence error ellipses for 2FGL J0322.4−3717 and 3FGL J0322.5−3721; the 3FGL source has the smaller ellipse. The dashed circle shows the 95% confidence error circle from our maximum-likelihood localization of the region as a single point source centered at position B. The other points (labeled C, D, E) are the locations of various sources and test sources, as detailed in the text and in Table 1.

Table 1
Fornax A Spatial Model Comparisons

Null Hypothesis	Alternative Hypothesis	dof[a]	$\Delta \log \mathcal{L}$	σ[b]	Sections
Point source (core location A)	Point source (best-fit location B)	2	0.6	0.6	2.1
Disk (best-fit location B, 0.°03 radius)	Disk (best-fit location B, 0.°33 radius)	1	17.3	5.9	2.2.1
Point source (best-fit location B)	Two point sources (locations D and E)	4	16.2	4.8	2.2.2
Point source (core location A)	Radio lobes template and point source (core location A)	2	19.8	6.0	2.2.3
Radio lobes template	Radio lobes template and point source (core location A)	2	0.7	0.7	2.2.3
Radio lobes template, rotated 90° CW	Radio lobes template	1	12.9	5.1	2.2.3
Radio lobes template, rotated 90° CCW	Radio lobes template	1	18.9	6.1	2.2.3
Radio lobes template	Radio lobes template and point source (location C)	4	7.0	2.7	2.2.3

Notes. Calculated using the likelihood ratio computation as described in Section 2.
[a] The difference in the number of degrees of freedom between the two hypotheses.
[b] The alternative hypotheses are preferred over the corresponding null hypotheses by the significances σ.

the distribution of significance values for the bins is Gaussian, indicating there are no significant systematic deviations from the ROI model. The map of residual counts shown in Figure 1 is cropped to a 1.°5 × 1.°5 region centered around the Fornax A core. The shape of the residuals suggests a non-circular morphology that resembles the known extended radio morphology. The contours of radio emission from a VLA 1.5 GHz image at 14″ resolution (Fomalont et al. 1989), with the radio core subtracted, are overlaid in Figure 1.

We also tested a model which included two separate point sources whose initial locations were chosen by eye based upon the residual counts. The locations of these two point sources were then optimized using `gtfindsrc`. The best-fit location of the western point source (labeled D in Figure 1) matches well the western lobe's centroid while the eastern point (labeled E in Figure 1) is offset from the centroid of the eastern lobe. The double point-source model is preferred over the single point-source model at a confidence level of 4.8σ. Table 1 details

Table 2
Fornax A LAT Spectral Fit Results

Model	TS	Energy Flux ($\times 10^{-12}$ erg cm^{-2} s^{-1})	Photon Index
Point (best-fit location B)	121	$5.34 \pm 0.78^{+0.03}_{-0.05\,\mathrm{sys}}$	$2.08 \pm 0.08 \pm 0.03_{\mathrm{sys}}$
Disk (best-fit location B, 0.°33 radius)	158	7 ± 1	1.99 ± 0.07
Radio lobes template	158	$7.57 \pm 1.05^{+0.06}_{-0.08\,\mathrm{sys}}$	$1.99 \pm 0.07^{+0.03}_{-0.04\,\mathrm{sys}}$
Two point sources, summed		6.6 ± 0.8	
West (location D)	37	2.9 ± 0.7	2.02 ± 0.13
East (location E)	51	3.7 ± 0.8	2.05 ± 0.11
Radio lobes template and point source (location C), summed		8 ± 1	
Radio lobes template	66	6 ± 1	1.97 ± 0.08
Point source (location C)	14	1.6 ± 0.6	2.01 ± 0.20

Note. Each fit was performed leaving normalization and spectral shape parameters of all sources free, except for the models for the diffuse background γ-rays which were fit with only normalization.

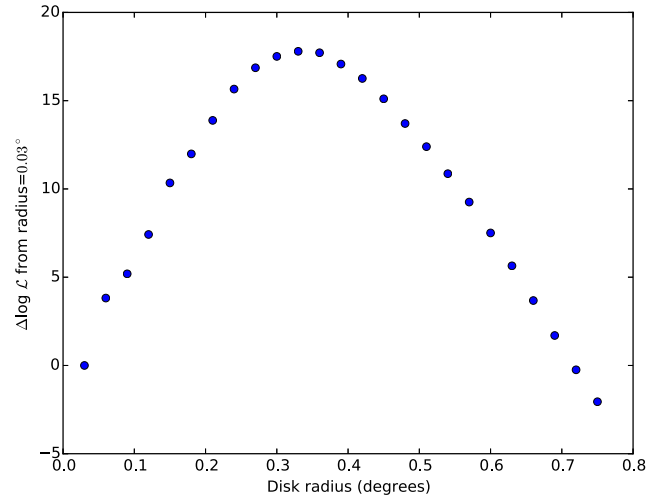

(a)

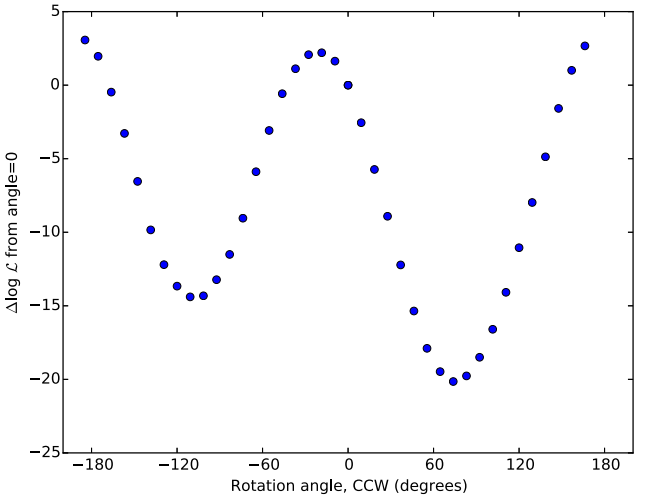

(b)

Figure 2. (a) $\Delta \log \mathcal{L}$ between a flat disk of radius 0.°03 (i.e., point-like) and flat disks of various radii. A cubic fit gives a maximum likelihood radius of $0.°33 \pm 0.°05$. The increase in $\mathcal{L}$ from 0.°03 to the maximum likelihood radius indicates the emission is not point-like. (b) $\Delta \log \mathcal{L}$ between the non-rotated radio lobe template and the template rotated around the central core indicating that the unrotated radio morphology is preferred.

these results and Table 2 lists the fit parameters. Note that the spectral index is statistically compatible with the single point-source model and for both point sources in the double point-source model.

2.2.3. Radio-motivated Tests for Morphology

Assuming that the same electron energy distribution (EED) determined from the radio emission scatters optical EBL photons to produce γ-rays, then a reasonable guess for the γ-ray morphology should be the observed radio structure. The lobes of Fornax A were found to emit non-thermal IC scattered X-rays, with excellent spatial coincidence to the radio structure produced by synchrotron-emitting relativistic electrons (Feigelson et al. 1995). Diffuse hard X-ray emission associated with the east lobe has been confirmed with *XMM-Newton* (Isobe et al. 2006), implying the magnetic field is reasonably uniform, further supporting the expectation that the γ-rays should match the radio morphology. Under these circumstances, as was observed in Centaurus A (Abdo et al. 2010), the relativistic electrons will trace the γ-ray emission (Georganopoulos et al. 2008). These assumptions could be incorrect; however, for the purpose of constraining the EBL with the γ-ray flux, using the radio structure is the best choice for the spatial distribution. Physically, Fornax A images from the *Wilkinson Microwave Anisotropy Probe* (*WMAP*) might be a better choice of template for the γ-ray emission because the synchrotron radiation within ~23–94 GHz should be originating from the same band of relativistic electrons that IC scatter into ~0.1–10 GeV γ-rays. We revisit this topic later in the section.

We created a spatial template of the lobe emission using VLA 1.5 GHz radio data (Fomalont et al. 1989), which offers a more-than-adequate spatial resolution of 14″. Both the central core of Fornax A and various radio point sources inside the lobe structure were manually removed from the spatial template, the former by reduction to zero and the latter by interpolation of the adjacent lobe-dominated flux. The central core was reduced to zero because the lobes do not overlap with the central core (Ekers et al. 1983). We found this template in addition to a point-source model of the core is preferred over just the point source at the core with a confidence of 6.0σ ($\Delta \log \mathcal{L} = 19.8$, 2 degrees of freedom). However, this combined model is preferred over the lobes template alone by only 0.7σ. Moreover, in the combined point-source-and-lobes template fit only 14% of the energy flux is assigned to the core point source. See Tables 1 and 2 for more information. We consider this as evidence that the γ-ray emission from the core

of Fornax A is insignificant. Minimal γ-ray flux from the central core is expected, as it is assumed to be synchrotron self-Compton, and the radio flux from the core has been reported to be relatively weak compared to the luminous galaxy lobes (Geldzahler & Fomalont 1984).

In order to test the uniqueness of the radio template morphology and its rotational symmetry, we rotated the template around the central core in increments of 9.°2 and computed the likelihood at each one. The results from this test are shown in Figure 2(b) and indicate that the template in its original orientation is preferred. In particular, we see the original orientation is a better model than the one rotated 90° clockwise with 5.1σ confidence ($\Delta \log \mathcal{L} = 12.9$, 1 degree of freedom) and 90° counterclockwise with 6.1σ confidence ($\Delta \log \mathcal{L} = 18.9$, 1 degree of freedom). The maximum likelihood rotation was $-20° \pm 10.°$ Additionally, our plot of $\log \mathcal{L}$ over template rotation angle shows a sinusoidal profile with a similar peak in likelihood around 180° as around 0°. This degeneracy indicates that the data are not constraining enough to statistically differentiate the lobes. Modeling the lobes as separate point sources (see Section 2.2.2) results in the measurement of similar fluxes and spectral shapes for the two regions, but this is at odds with radio observations of the lobes. According to the 1.5 GHz VLA observation (Fomalont et al. 1989), the west lobe has about twice the total flux than the east. In fact, the two point-source γ-ray analysis indicated the east lobe may be slightly brighter (but is within the statistical errors). This disagreement may be a symptom of our use of 1.5 GHz VLA data instead of the very similar but more physically motivated ~23–94 GHz *WMAP* data as a spatial template for the γ-rays. Indeed, the flux ratio of west to east is ~1.3 in the *WMAP* 41 and 61 GHz maps (Georganopoulos et al. 2008), closer to the γ-ray result. However, Fornax A is at the resolving power of the LAT in this analysis and the PSF is broad enough (~0.°8 radius at 1 GeV) that fine scale changes would be smoothed out and indistinguishable from the original, and small changes in the flux ratio between the lobes should leave the average flux nearly the same. This is highlighted by the similarity in overall likelihood we observe between 0° and 180° rotations of the 1.5 GHz VLA template, where the rotation of 180° is identical to a flux ratio of ~0.5. In addition, even when using the spatial morphology of a single point source, the flux is nearly consistent with the radio template flux (see Section 2.1).

With the aim of testing the region for the possibility of a contaminating background γ-ray source, we added a point source to the lobes template model and optimized its position using `gtfindsrc`. The optimized position of this point source (labeled C in Figure 1) was R.A. $= 50.°67$, decl. $= -37.°46$ with a 95% confidence error circle radius of 0.°42 (large enough to encompass the whole Fornax A emission region). The resulting fit was marginally preferred over the lobes template alone with 2.7σ significance. Therefore, we do not consider any contribution from a background point source to be significant.

2.3. Spectral and Temporal Analysis

In the following we assume the radio morphology template (without any core contribution) is the best description of the Fornax A γ-ray emission. The likelihood ratio technique cannot quantify whether the radio template is statistically preferred with respect to the best-fit disk model because these models are not nested. However, the radio template is the physically motivated model based on the leptonic scenario of γ-ray production. Further, the rotation study presented above indicates a preferred axis of the γ-ray emission which mimics the elongated emission observed at radio frequencies, in turn supporting the similarity between the γ-ray and radio emission morphology.

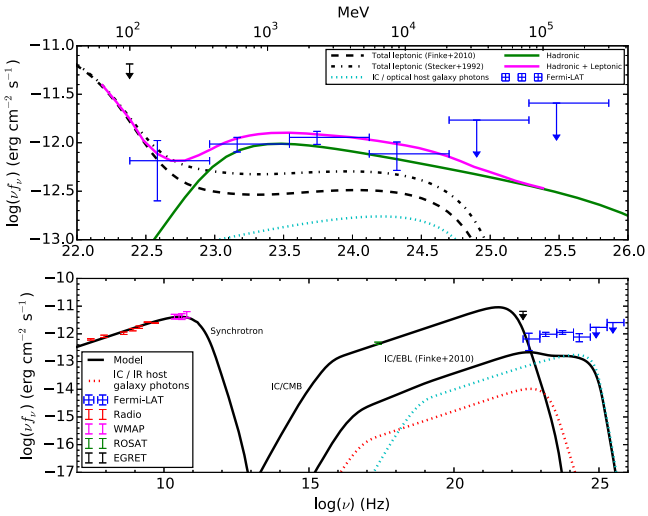

Figure 3. Broadband SED of the lobes of Fornax A (bottom panel) and detailed view of the high-energy part of the SED (top panel). As in Georganopoulos et al. (2008), we used archival measurements of the total lobe radio flux densities (shown in red) from Finlay & Jones (1973), Cameron (1971), Jones & McAdam (1992), Ekers et al. (1983), Bolton & Shimmins (1973), and Kühr et al. (1981), as collected by Isobe et al. (2006), replacing an extrapolated 100 MHz data point from Finlay & Jones (1973) with an 86 MHz measurement (Mills et al. 1960). The 3 year integrated *WMAP* data are shown in magenta (Hinshaw et al. 2007), and X-ray data from *ROSAT* (Feigelson et al. 1995) are shown in green. The LAT data points from this study are shown in blue. The black upper limit point is from EGRET (Cillis et al. 2004). The black solid lines from left to right show the synchrotron ($<10^{13}$ Hz), IC/CMB ($>10^{13}$ Hz), and IC/EBL (on the assumption of the model of Finke et al. (2010)) flux models ($>10^{15}$ Hz). The dashed black line shows the IC/EBL flux models assuming the fast evolution model of Stecker et al. (1992). The dotted red and cyan lines show the IC upscattered host galaxy photon flux from infrared and optical, respectively. The solid green line shows the hadronic model flux, while the solid magenta line shows the combined hadronic and leptonic model flux.

We tested several broadband spectral models (log-parabola, broken power law, and broken power law with an exponential cutoff), and found none were significantly preferred over the single power law. Then, we measured spectral points by fitting each of 6 equal logarithmically spaced energy bins from 0.1 to 300 GeV to a power law and optimized the flux normalizations by maximizing the likelihood function. In each bin, the normalization parameters for all sources were free, and all other parameters were fixed to the values obtained from the broadband fit. These spectral data points are shown in Figure 3 and Table 3. The source is detected in 4 of the 6 spectral bins with TS > 5, and 95% confidence upper limits were calculated for the two lower-significance bins (at the highest energies).

To test the γ-ray variability over the 6.1 year period, we made a 0.1–300 GeV light curve in time bins of 185 days, which was found to be the smallest possible timescale while maintaining a reasonable significance of detection in the majority of bins. For each time interval, the emission associated with Fornax A was fit to a single point source (positioned at the best-fit location B in Figure 1), as we expected any potential

Table 3
Fornax A Total Lobe LAT Spectral Flux

Bin Energy Range (GeV)	Energy Flux ($\times 10^{-12}$ erg cm^{-2} s^{-1})	TS
0.10–0.38	0.7 ± 0.4	6.1
0.38–1.4	1.0 ± 0.2	49
1.4–5.5	1.1 ± 0.2	87
5.5–21	0.8 ± 0.2	22
21–79[a]	<1.7	3.5
79–300[a]	<2.6	4.3

Notes. Assuming radio lobes template spatial model.
[a] 95% confidence upper limits.

variable emission to be associated with a point source at the core and not the lobes. All sources included in the 6.1 year analysis were fit with all spectral shape parameters fixed to their optimized values from the full fit, while all normalizations were left free. Upper limits were calculated for time bins within which the TS fell below 4 ($<2\sigma$). The significance of variability was determined following the method described in Nolan et al. (2012). Our analysis yielded a 1.3σ confidence that the emission is variable, and so we conclude that we do not observe significant variability.

3. RESULTS AND DISCUSSION

Our *Fermi*-LAT study of the region around Fornax A consistently shows that, under all tests performed, the γ-ray emission region is significantly extended and the most likely spatial distribution is delineated by the radio lobes. Using a size-optimized flat disk model, extension beyond a point source was found to be significant at 5.9σ confidence, with a preferred radius of $0\overset{\circ}{.}33 \pm 0\overset{\circ}{.}05$. Modeling the emission as two point sources results in a western point source well matched to the radio lobe centroid and an eastern point source offset from the eastern lobe. This model is preferred over a single point source at the 4.8σ level. Furthermore, using the 1.5 GHz VLA radio morphology (Fomalont et al. 1989) as a template in combination with a central core point source results in a significantly greater likelihood than the point source alone with 6.0σ confidence. Contamination from the core is determined to be at most 14% based on a likelihood fit with the radio lobes template and a point source at the core location. While it is difficult to determine the exact morphology of the γ-ray emission, our study shows that it cannot be fully described as a point-like source.

A few scenarios could explain the offset γ-ray point-source localization seen in the 3FGL and in the single point-source analysis presented here. First, since we now know the emission is extended (or at least not point-like), to use a point-source model to localize the emission is to start with a false assumption. The distribution of the γ-ray emitting regions may not be uniform across the lobe structure and thus would not result in a symmetric distribution of γ-ray emission. Second, based upon the offset eastern lobe point-source localization (point E in Figure 1), the existence of a background γ-ray source is not ruled out. However, adding a point source to the lobes template model and localizing with `gtfindsrc` yields only a slightly better fit at the 2.7σ level (see point C in Figure 1). We also find no evidence for variability in this source over ~6 years of observations. Variability might support the presence of a common background source such as a blazar. We note that another potential source that has been investigated in this region is the Fornax cluster (Ando & Nagai 2012; Ackermann et al. 2014) whose center lies $3\overset{\circ}{.}6$ northeast of the Fornax A core, and may be contributing contaminating γ-ray flux from various cluster constituents. However, no galaxy cluster has been detected in γ-rays so far.

Fermi-LAT data have been previously used by McKinley et al. (2015) to study Fornax A. They reported a photon flux above 100 MeV of 6.7×10^{-9} ph cm^{-2} s^{-1} using a point source spatial model, and our finding using the lobes template was close at $(5.7 \pm 0.9) \times 10^{-9}$ ph cm^{-2} s^{-1}. Our study establishes for the first time spatial extension of Fornax A in γ-rays, and distinguishes between γ-ray contributions from the core and lobes. This result was enabled thanks to the improvements brought about by the new Pass 8 event reconstruction, rather than the marginal increase in exposure time (i.e., 6 years of data in our study instead of 5 years in theirs).

3.1. Leptonic Modeling

We model the γ-ray emission following Georganopoulos et al. (2008), in which the relativistic electrons in the lobes of the radio galaxy are IC scattered off of CMB and EBL photons. For a given EED of the lobes, the resulting IC emission will consist of a lower-energy component due to CMB photons, as well as two components at higher energy due to the cosmic infrared and optical backgrounds (CIB and COB, respectively). While the EBL energy density is only a few percent that of the CMB, the resulting IC spectrum due to CIB and COB photons will be shifted in frequency by $\gamma_{\rm max}^2$, where $\gamma_{\rm max}$ is the maximum Lorentz factor of the EED. The EED used in this model is a broken power law that breaks at $\gamma_{\rm break} = 1.3 \times 10^5$ from an electron index of 2.3 to a much larger value to mimic a cutoff. This break was chosen so as to not overproduce the emission in the lowest-energy LAT band. With peak wavelengths of $\lambda \sim 100$ μm and ~ 1 μm for the CIB and COB, the resulting IC spectrum will be shifted in frequency by factors of ~10 and 1000, respectively from that of the upscattered CMB.

This model is shown along with the γ-ray spectral energy distribution and the radio-to-sub-mm measurements of the total emission from the lobes presented in Georganopoulos et al. (2008) in Figure 3. Note that because Fornax A is an extended source in other wavelengths as well, care must be taken in defining the spatial structure in all wavelengths in order to draw meaningful comparisons. This model makes use of currently available *total* lobe fluxes. *WMAP* and Planck fluxes reported by McKinley et al. (2015) were obtained using resolution-dependent apertures that did not fully enclose the extent of the synchrotron lobe emission. We assumed a lobe magnetic field strength of 1.65 μG, constrained to the X-ray flux data point, and we include photon contributions from the host galaxy following Georganopoulos et al. (2008). The extracted spectral data points do not appear to match the predicted model shape based on IC/EBL emission alone. Fully accounting for the *Fermi*-LAT observed fluxes under the IC/EBL hypothesis alone would imply an EBL level that is even higher than the Stecker model (Stecker et al. 1992), which was ruled out by Ackermann et al. (2012). Consequently, the applied leptonic model cannot completely explain the observed emission. The model relies upon the assumption that all of the X-ray flux observed from the lobes is created by IC/CMB scattering to

obtain the magnetic field strength. If some amount of the X-ray flux is thermal emission (as reported by Seta et al. 2013), our expected IC/EBL level would decrease, creating further discrepancy between model and data.

As discussed in Section 2.2.3, a more physically motivated choice of spatial template would be the higher-frequency *WMAP* data. However, the resulting changes in flux and spectral shape should be within the statistical errors of our current results, and therefore should not alter our result that the flux exceeds the leptonic model of the Fornax A lobes.

Note that the intensity of the IC contribution from the host galaxy photons of Fornax A is comparable to that of the EBL photons in the lobes, and it actually dominates at higher energies (>1 GeV, see Figure 3). This differs from the case of Centaurus A, wherein the predicted EBL photon intensity is roughly five times that of the starlight (Abdo et al. 2010). Were it true that host galaxy photons dominate in Fornax A, the expected spatial distribution of γ-rays from the lobes would not be uniform, with brighter emission nearer the center and less away from the core. Testing for this feature requires spatial resolution that is beyond the capabilities of the LAT with current statistics.

3.2. Hadronic Modeling

The problem of the model not fitting the γ-ray spectrum in Fornax A may be solved by an additional contribution from hadronic cosmic rays interacting within the lobes, as found by McKinley et al. (2015). We created a model of hadronic emission (proton–proton interactions) assuming a total emitting volume of 7×10^{70} cm^3 and a uniform distribution of thermal gas with number density 3×10^{-4} cm^{-3} following Seta et al. (2013), and a power-law cosmic-ray spectrum with energy index 2.3 extending from ~3 GeV up to more than 10 TeV. Modeling the γ-rays as entirely hadronic in origin requires a large total cosmic-ray energy of $\sim 1 \times 10^{61}$ erg, which is twice the observed energy of $\sim 5 \times 10^{60}$ erg in the lobes of comparable radio galaxy Hydra A (Abramowski et al. 2012) and very high compared to an estimate of $\sim 5 \times 10^{58}$ erg in the outburst that is assumed to have created the lobes of Fornax A (Lanz et al. 2010). We then subtracted the lowest IC/EBL model (Finke et al. 2010) from our LAT spectral points and fit the residual flux as hadronic emission, and found we could achieve a reasonable fit, shown in Figure 3. The resulting cosmic-ray pressure fitted from this residual flux is $\sim 2 \times 10^{-11}$ dyn cm^{-2} and the total energy stored in cosmic rays is $\sim 5 \times 10^{60}$ erg. This total energy is similar to that of Hydra A (Abramowski et al. 2012) and closer to an estimate of the total energy in the Fornax A lobes (Lanz et al. 2010). This result agrees with analogous calculations by McKinley et al. (2015), in which the discrepancy is explained by suggesting the emission is primarily hadronic and localized to relatively denser sub-structures within the lobes, thereby decreasing the effective emitting volume.

4. CONCLUSIONS

We report the first *Fermi*-LAT detection of extended γ-ray emission from the radio galaxy Fornax A using 6.1 years of *Fermi*-LAT data. We conclude that a point-source spatial model is insufficient to describe the γ-ray emission, and our analysis indicates it is likely the emission originates in the lobes. We investigated the origin of the extended emission by assuming leptonic emission that arises due to IC scattering of EBL photons off of relativistic electrons in the radio lobes. This leptonic modeling underestimates the observed γ-ray emission for any current EBL estimate, consistent with the recent findings by McKinley et al. (2015), even after accounting for the additional contribution of IC emission off of the host galaxy light. A hadronic-only model (proton–proton interactions) requires implausibly large total cosmic-ray energy when compared to an estimate of the Fornax A outburst assumed to have created the lobes (Lanz et al. 2010), and this problem can be alleviated by invoking denser sub-structures in the lobes (McKinley et al. 2015). When we assume the lowest EBL model (Finke et al. 2010) and fit the residual γ-ray flux as hadronic production, our fit yields a total cosmic-ray energy of $\sim 5 \times 10^{60}$ erg, matching well with the Hydra A energy (Abramowski et al. 2012), but still at least 100 times greater than the estimated total energy in the Fornax A lobes (Lanz et al. 2010). Thus, even the combined leptonic and hadronic scenario may not be able to explain the γ-ray lobe emission. Given our current understanding of the content of the radio lobes and the EBL, some contribution from leptonic processes must exist. If it is true that there is a γ-ray component other than leptonic in Fornax A, we should expect to observe such a component in other nearby radio galaxies as well.

Our spatial analysis hinted at the existence of a background γ-ray source (C in Figure 1). We re-evaluated the SED of Fornax A including this source in the model, but we found this background source addition is only marginally preferred and cannot fully make up the difference between the data and the IC/EBL model. In any case, γ-ray contamination from an unresolved background source or the Fornax cluster could be present.

Our modeling was done using previously published multi-wavelength data. Further analysis in other wavelengths in the future will yield a more definitive picture of the SED. More detailed observations, such as with the hard X-ray telescope *NuSTAR*, would help determine if the X-ray emission is contaminated by thermal processes (Seta et al. 2013), which would test our initial assumptions that the radio data traces the X-rays and γ-rays, and that the X-rays could be used to constrain the lobe magnetic field. *Fermi*-LAT analysis at even lower energies (below 100 MeV) may provide more information about the IC/CMB component (Cheung 2007). Potentially with greater statistics, the *Fermi*-LAT could extend the lobes' detection to higher energies and additionally observe the effect of the host-galaxy photons on the spatial distribution of γ-rays in the Fornax A lobes.

The *Fermi*-LAT Collaboration acknowledges generous ongoing support from a number of agencies and institutes that have supported both the development and the operation of the LAT as well as scientific data analysis. These include the National Aeronautics and Space Administration and the Department of Energy in the United States, the Commissariat à l'Energie Atomique and the Centre National de la Recherche Scientifique/Institut National de Physique Nucléaire et de Physique des Particules in France, the Agenzia Spaziale Italiana and the Istituto Nazionale di Fisica Nucleare in Italy, the Ministry of Education, Culture, Sports, Science and Technology (MEXT), High Energy Accelerator Research Organization (KEK) and Japan Aerospace Exploration Agency (JAXA) in Japan, and the K. A. Wallenberg Foundation, the

Swedish Research Council and the Swedish National Space Board in Sweden.

Additional support for science analysis during the operations phase is gratefully acknowledged from the Istituto Nazionale di Astrofisica in Italy and the Centre National d'Études Spatiales in France.

Facility: Fermi.

REFERENCES

Abdo, A. A., Ackermann, M., Ajello, M., et al. (*Fermi*-LAT collaboration) 2010, Sci, 328, 725
Abramowski, A., Acero, F., Aharonian, F., et al. (H.E.S.S. collaboration) 2012, A&A, 545, A103
Acero, F., Ackermann, M., Ajello, M., et al. (*Fermi*-LAT collaboration) 2015, ApJS, 218, 23
Ackermann, M., Ajello, M., Albert, A., et al. (*Fermi*-LAT collaboration) 2014, ApJ, 787, 18
Ackermann, M., Ajello, M., Allafort, A., et al. (*Fermi*-LAT collaboration) 2012, Sci, 338, 1190
Ackermann, M., Ajello, M., Atwood, W., et al. (*Fermi*-LAT collaboration) 2015, ApJ, 810, 14
Ando, S., & Nagai, D. 2012, JCAP, 7, 017
Atwood, W. B., Abdo, A. A., Ackermann, M., et al. (*Fermi*-LAT collaboration) 2009, ApJ, 697, 1071
Bolton, J. G., & Shimmins, A. J. 1973, AuJPA, 30, 1
Cameron, M. J. 1971, MNRAS, 152, 439
Cheung, C. C. 2007, ASPC, 373, 255
Cillis, A. N., Hartman, R. C., & Bertsch, D. L. 2004, ApJ, 601, 142
Croston, J. H., Hardcastle, M. J., Harris, D. E., et al. 2005, ApJ, 626, 733
Ekers, R. D., Goss, W. M., Wellington, K. J., et al. 1983, A&A, 127, 361
Feigelson, E. D., Laurent-Muehleisen, S. A., Kollgaard, R. I., et al. 1995, ApJL, 449, L149
Finke, J. D., Razzaque, S., & Dermer, C. D. 2010, ApJ, 712, 238
Finlay, E. A., & Jones, B. B. 1973, AuJPh, 26, 389
Fomalont, E. B., Ebneter, K. A., van Breugel, W. J. M., & Ekers, R. D. 1989, ApJ, 346, 17
Geldzahler, B. J., & Fomalont, E. B. 1984, AJ, 89, 1650
Georganopoulos, M., Sambruna, R. M., Kazanas, D., et al. 2008, ApJL, 686, L5
Harris, D. E., & Grindlay, J. E. 1979, MNRAS, 188, L25
Hinshaw, G., Nolta, M. R., Bennett, C. L., et al. 2007, ApJS, 170, 288
Isobe, N., Makishima, K., Tashiro, M., et al. 2006, ApJ, 645, 256
Isobe, N., Seta, H., & Tashiro, M. S. 2011, PASJ, 63, S947
Jones, P. A., & McAdam, W. B. 1992, ApJS, 80, 137
Kaneda, H., Tashiro, M., Ikebe, Y., et al. 1995, ApJL, 453, L13
Kataoka, J., & Stawarz, Ł 2005, ApJ, 622, 797
Katsuta, J., Tanaka, Y. T., Stawarz, L., et al. 2013, A&A, 550, A66
Kim, D., & Fabbiano, G. 2003, ApJ, 586, 826
Kühr, H., Witzel, A., Pauliny-Toth, I. I. K., & Nauber, U. 1981, A&AS, 45, 367
Lande, J., Ackermann, M., Allafort, A., et al. 2012, ApJ, 756, 5
Lanz, L., Jones, C., Forman, W. R., et al. 2010, ApJ, 721, 1702
Madore, B. F., Freedman, W. L., Silbermann, N., et al. 1999, ApJ, 515, 29
Mattox, J. R., Bertsch, D. L., Chiang, J., et al. 1996, ApJ, 461, 396
McKinley, B., Yang, R., López-Caniego, M., et al. 2015, MNRAS, 446, 3478
Mills, B. Y., Slee, O. B., & Hill, E. R. 1960, AuJPh, 13, 676
Nolan, P. L., Abdo, A. A., Ackermann, M., et al. (*Fermi*-LAT collaboration) 2012, ApJS, 199, 31
O'Sullivan, S. P., Feain, I. J., McClure-Griffiths, N. M., et al. 2013, ApJ, 764, 162
Seta, H., Tashiro, M. S., & Inoue, S. 2013, PASJ, 65, 106
Sgrò, C. 2014, Proc. SPIE, 9144, 91443K
Stawarz, Ł, Tanaka, Y. T., Madejski, G., et al. 2013, ApJ, 766, 48
Stecker, F. W., de Jager, O. C., & Salamon, M. H. 1992, ApJL, 390, L49
Takeuchi, Y., Kataoka, J., Stawarz, L., et al. 2012, ApJ, 749, 66
Tashiro, M. S., Isobe, N., Seta, H., Matsuta, K., & Yaji, Y. 2009, PASJ, 61, 327
Wilks, S. S. 1938, AMS, 1, 60